

Study of  $\phi$  meson production in  $p+\text{Al}$ ,  $p+\text{Au}$ ,  $d+\text{Au}$ , and  ${}^3\text{He}+\text{Au}$  collisions at  
 $\sqrt{s_{NN}} = 200 \text{ GeV}$

U. Acharya,<sup>20</sup> A. Adare,<sup>12</sup> C. Aidala,<sup>42</sup> N.N. Ajitanand,<sup>61,\*</sup> Y. Akiba,<sup>56,57,†</sup> M. Alfred,<sup>22</sup> V. Andrieux,<sup>42</sup>  
N. Apadula,<sup>27,62</sup> H. Asano,<sup>34,56</sup> B. Azmoun,<sup>7</sup> V. Babintsev,<sup>23</sup> M. Bai,<sup>6</sup> N.S. Bandara,<sup>40</sup> B. Bannier,<sup>62</sup> K.N. Barish,<sup>8</sup>  
S. Bathe,<sup>5,57</sup> A. Bazilevsky,<sup>7</sup> M. Beaumier,<sup>8</sup> S. Beckman,<sup>12</sup> R. Belmont,<sup>12,42,49</sup> A. Berdnikov,<sup>59</sup> Y. Berdnikov,<sup>59</sup>  
L. Bichon,<sup>67</sup> B. Blankenship,<sup>67</sup> D.S. Blau,<sup>33,46</sup> J.S. Bok,<sup>48</sup> V. Borisov,<sup>59</sup> K. Boyle,<sup>57</sup> M.L. Brooks,<sup>36</sup>  
J. Bryslawskyj,<sup>5,8</sup> V. Bumazhnov,<sup>23</sup> S. Campbell,<sup>13,27</sup> V. Canoa Roman,<sup>62</sup> R. Cervantes,<sup>62</sup> C.-H. Chen,<sup>57</sup>  
M. Chiu,<sup>7</sup> C.Y. Chi,<sup>13</sup> I.J. Choi,<sup>24</sup> J.B. Choi,<sup>29,\*</sup> T. Chujo,<sup>66</sup> Z. Citron,<sup>68</sup> M. Connors,<sup>20,57</sup> R. Corliss,<sup>62</sup>  
Y. Corrales Morales,<sup>36</sup> N. Cronin,<sup>44,62</sup> M. Csanád,<sup>16</sup> T. Csörgő,<sup>41,69</sup> T.W. Danley,<sup>50</sup> A. Datta,<sup>47</sup> M.S. Daugherty,<sup>1</sup>  
G. David,<sup>7,62</sup> C.T. Dean,<sup>36</sup> K. DeBlasio,<sup>47</sup> K. Dehmelt,<sup>62</sup> A. Denisov,<sup>23</sup> A. Deshpande,<sup>57,62</sup> E.J. Desmond,<sup>7</sup>  
A. Dion,<sup>62</sup> P.B. Diss,<sup>39</sup> D. Dixit,<sup>62</sup> J.H. Do,<sup>70</sup> V. Doomra,<sup>62</sup> A. Drees,<sup>62</sup> K.A. Drees,<sup>6</sup> J.M. Durham,<sup>36</sup> A. Durum,<sup>23</sup>  
H. En'yo,<sup>56</sup> A. Enokizono,<sup>56,58</sup> R. Esha,<sup>62</sup> S. Esumi,<sup>66</sup> B. Fadem,<sup>44</sup> W. Fan,<sup>62</sup> N. Feege,<sup>62</sup> D.E. Fields,<sup>47</sup>  
M. Finger, Jr.,<sup>9</sup> M. Finger,<sup>9</sup> D. Firak,<sup>62</sup> D. Fitzgerald,<sup>42</sup> S.L. Fokin,<sup>33</sup> J.E. Frantz,<sup>50</sup> A. Franz,<sup>7</sup> A.D. Frawley,<sup>19</sup>  
Y. Fukuda,<sup>66</sup> P. Gallus,<sup>14</sup> C. Gal,<sup>62</sup> P. Garg,<sup>3,62</sup> H. Ge,<sup>62</sup> M. Giles,<sup>62</sup> F. Giordano,<sup>24</sup> A. Glenn,<sup>35</sup> Y. Goto,<sup>56,57</sup>  
N. Grau,<sup>2</sup> S.V. Greene,<sup>67</sup> M. Grosse Perdekamp,<sup>24</sup> T. Gunji,<sup>11</sup> H. Guragain,<sup>20</sup> T. Hachiya,<sup>45,56,57</sup> J.S. Haggerty,<sup>7</sup>  
K.I. Hahn,<sup>17</sup> H. Hamagaki,<sup>11</sup> H.F. Hamilton,<sup>1</sup> J. Hanks,<sup>62</sup> S.Y. Han,<sup>17,32</sup> M. Harvey,<sup>64</sup> S. Hasegawa,<sup>28</sup>  
T.O.S. Haseler,<sup>20</sup> K. Hashimoto,<sup>56,58</sup> T.K. Hemmick,<sup>62</sup> X. He,<sup>20</sup> J.C. Hill,<sup>27</sup> K. Hill,<sup>12</sup> A. Hodges,<sup>20</sup> R.S. Hollis,<sup>8</sup>  
K. Homma,<sup>21</sup> B. Hong,<sup>32</sup> T. Hoshino,<sup>21</sup> N. Hotvedt,<sup>27</sup> J. Huang,<sup>7</sup> K. Imai,<sup>28</sup> M. Inaba,<sup>66</sup> A. Iordanova,<sup>8</sup>  
D. Isenhower,<sup>1</sup> D. Ivanishchev,<sup>54</sup> B.V. Jacak,<sup>62</sup> M. Jezghani,<sup>20</sup> X. Jiang,<sup>36</sup> Z. Ji,<sup>62</sup> B.M. Johnson,<sup>7,20</sup> D. Jouan,<sup>52</sup>  
D.S. Jumper,<sup>24</sup> S. Kanda,<sup>11</sup> J.H. Kang,<sup>70</sup> D. Kapukchyan,<sup>8</sup> S. Karthas,<sup>62</sup> D. Kawall,<sup>40</sup> A.V. Kazantsev,<sup>33</sup>  
J.A. Key,<sup>47</sup> V. Khachatryan,<sup>62</sup> A. Khanzadeev,<sup>54</sup> A. Khatiwada,<sup>36</sup> B. Kimelman,<sup>44</sup> C. Kim,<sup>8,32</sup> D.J. Kim,<sup>30</sup>  
E.-J. Kim,<sup>29</sup> G.W. Kim,<sup>17</sup> M. Kim,<sup>60</sup> T. Kim,<sup>17</sup> D. Kincses,<sup>16</sup> A. Kingan,<sup>62</sup> E. Kistenev,<sup>7</sup> R. Kitamura,<sup>11</sup>  
J. Klatsky,<sup>19</sup> D. Kleinjan,<sup>8</sup> P. Kline,<sup>62</sup> T. Koblesky,<sup>12</sup> B. Komkov,<sup>54</sup> D. Kotov,<sup>54,59</sup> L. Kovacs,<sup>16</sup> S. Kudo,<sup>66</sup>  
B. Kurgiy,<sup>16</sup> K. Kurita,<sup>58</sup> M. Kurosawa,<sup>56,57</sup> Y. Kwon,<sup>70</sup> J.G. Lajoie,<sup>27</sup> D. Larionova,<sup>59</sup> A. Lebedev,<sup>27</sup> S. Lee,<sup>70</sup>  
S.H. Lee,<sup>27,42,62</sup> M.J. Leitch,<sup>36</sup> Y.H. Leung,<sup>62</sup> N.A. Lewis,<sup>42</sup> S.H. Lim,<sup>36,55,70</sup> M.X. Liu,<sup>36</sup> X. Li,<sup>10</sup> X. Li,<sup>36</sup>  
V.-R. Loggins,<sup>24</sup> D.A. Loomis,<sup>42</sup> K. Lovasz,<sup>15</sup> D. Lynch,<sup>7</sup> S. Lökös,<sup>16</sup> T. Majoros,<sup>15</sup> Y.I. Makdisi,<sup>6</sup> M. Makek,<sup>71</sup>  
A. Manion,<sup>62</sup> V.I. Manko,<sup>33</sup> E. Mannel,<sup>7</sup> M. McCumber,<sup>36</sup> P.L. McGaughey,<sup>36</sup> D. McGlinchey,<sup>12,36</sup> C. McKinney,<sup>24</sup>  
A. Meles,<sup>48</sup> M. Mendoza,<sup>8</sup> A.C. Mignerey,<sup>39</sup> A. Milov,<sup>68</sup> D.K. Mishra,<sup>4</sup> J.T. Mitchell,<sup>7</sup> M. Mitrankova,<sup>59</sup>  
Iu. Mitrankov,<sup>59</sup> G. Mitsuka,<sup>31,57</sup> S. Miyasaka,<sup>56,65</sup> S. Mizuno,<sup>56,66</sup> A. Mohamed,<sup>15</sup> A.K. Mohanty,<sup>4</sup>  
M.M. Mondal,<sup>62</sup> P. Montuenga,<sup>24</sup> T. Moon,<sup>32,70</sup> D.P. Morrison,<sup>7</sup> T.V. Moukhanova,<sup>33</sup> B. Mulilo,<sup>32,56,72</sup>  
T. Murakami,<sup>34,56</sup> J. Murata,<sup>56,58</sup> A. Mwai,<sup>61</sup> K. Nagai,<sup>65</sup> K. Nagashima,<sup>21</sup> T. Nagashima,<sup>58</sup> J.L. Nagle,<sup>12</sup>  
M.I. Nagy,<sup>16</sup> I. Nakagawa,<sup>56,57</sup> H. Nakagomi,<sup>56,66</sup> K. Nakano,<sup>56,65</sup> C. Natrass,<sup>63</sup> S. Nelson,<sup>18</sup> P.K. Netrakanti,<sup>4</sup>  
T. Niida,<sup>66</sup> S. Nishimura,<sup>11</sup> R. Nouicer,<sup>7,57</sup> N. Novitzky,<sup>30,62,66</sup> T. Novák,<sup>41,69</sup> G. Nukazuka,<sup>56,57</sup> A.S. Nyanin,<sup>33</sup>  
E. O'Brien,<sup>7</sup> C.A. Ogilvie,<sup>27</sup> J. Oh,<sup>55</sup> J.D. Orjuela Koop,<sup>12</sup> M. Orosz,<sup>73</sup> J.D. Osborn,<sup>42,51</sup> A. Oskarsson,<sup>37</sup>  
G.J. Ottino,<sup>47</sup> K. Ozawa,<sup>31,66</sup> R. Pak,<sup>7</sup> V. Pantuev,<sup>25</sup> V. Papavassiliou,<sup>48</sup> J.S. Park,<sup>60</sup> S. Park,<sup>43,56,60,62</sup>  
M. Patel,<sup>27</sup> S.F. Pate,<sup>48</sup> J.-C. Peng,<sup>24</sup> W. Peng,<sup>67</sup> D.V. Perepelitsa,<sup>7,12</sup> G.D.N. Perera,<sup>48</sup> D.Yu. Peressounko,<sup>33</sup>  
C.E. PerezLara,<sup>62</sup> J. Perry,<sup>27</sup> R. Petti,<sup>7,62</sup> M. Phipps,<sup>7,24</sup> C. Pinkenburg,<sup>7</sup> R. Pinson,<sup>1</sup> R.P. Pisani,<sup>7</sup> M. Potekhin,<sup>7</sup>  
A. Pun,<sup>50</sup> M.L. Purschke,<sup>7</sup> P.V. Radzevich,<sup>59</sup> J. Rak,<sup>30</sup> N. Ramasubramanian,<sup>62</sup> B.J. Ramson,<sup>42</sup> I. Ravinovich,<sup>68</sup>  
K.F. Read,<sup>51,63</sup> D. Reynolds,<sup>61</sup> V. Riabov,<sup>46,54</sup> Y. Riabov,<sup>54,59</sup> D. Richford,<sup>5</sup> T. Rinn,<sup>24,27</sup> S.D. Rolnick,<sup>8</sup>  
M. Rosati,<sup>27</sup> Z. Rowan,<sup>5</sup> J.G. Rubin,<sup>42</sup> J. Runchey,<sup>27</sup> A.S. Safonov,<sup>59</sup> B. Sahlmueller,<sup>62</sup> N. Saito,<sup>31</sup> T. Sakaguchi,<sup>7</sup>  
H. Sako,<sup>28</sup> V. Samsonov,<sup>46,54</sup> M. Sarsour,<sup>20</sup> S. Sato,<sup>28</sup> B. Schaefer,<sup>67</sup> B.K. Schmoll,<sup>63</sup> K. Sedgwick,<sup>8</sup> R. Seidl,<sup>56,57</sup>  
A. Sen,<sup>27,63</sup> R. Seto,<sup>8</sup> P. Sett,<sup>4</sup> A. Sexton,<sup>39</sup> D. Sharma,<sup>62</sup> I. Shein,<sup>23</sup> Z. Shi,<sup>36</sup> M. Shibata,<sup>45</sup> T.-A. Shibata,<sup>56,65</sup>  
K. Shigaki,<sup>21</sup> M. Shimomura,<sup>27,45</sup> T. Shioya,<sup>66</sup> P. Shukla,<sup>4</sup> A. Sickles,<sup>7,24</sup> C.L. Silva,<sup>36</sup> D. Silvermyr,<sup>37,51</sup>  
B.K. Singh,<sup>3</sup> C.P. Singh,<sup>3</sup> V. Singh,<sup>3</sup> M. Slunečka,<sup>9</sup> K.L. Smith,<sup>19</sup> M. Snowball,<sup>36</sup> R.A. Soltz,<sup>35</sup> W.E. Sondheim,<sup>36</sup>  
S.P. Sorensen,<sup>63</sup> I.V. Sourikova,<sup>7</sup> P.W. Stankus,<sup>51</sup> M. Stepanov,<sup>40,\*</sup> S.P. Stoll,<sup>7</sup> T. Sugitate,<sup>21</sup> A. Sukhanov,<sup>7</sup>  
T. Sumita,<sup>56</sup> J. Sun,<sup>62</sup> Z. Sun,<sup>15</sup> J. Sziklai,<sup>69</sup> R. Takahama,<sup>45</sup> A. Taketani,<sup>56,57</sup> K. Tanida,<sup>28,57,60</sup>  
M.J. Tannenbaum,<sup>7</sup> S. Tarafdar,<sup>67,68</sup> A. Taranenko,<sup>46,61</sup> G. Tarnai,<sup>15</sup> R. Tieulent,<sup>20,38</sup> A. Timilsina,<sup>27</sup>  
T. Todoroki,<sup>56,57,66</sup> M. Tomášek,<sup>14</sup> C.L. Towell,<sup>1</sup> R. Towell,<sup>1</sup> R.S. Towell,<sup>1</sup> I. Tserruya,<sup>68</sup> Y. Ueda,<sup>21</sup> B. Ujvari,<sup>15</sup>  
H.W. van Hecke,<sup>36</sup> J. Velkovska,<sup>67</sup> M. Virius,<sup>14</sup> V. Vrba,<sup>14,26</sup> N. Vukman,<sup>71</sup> X.R. Wang,<sup>48,57</sup> Z. Wang,<sup>5</sup>  
Y. Watanabe,<sup>56,57</sup> Y.S. Watanabe,<sup>11,31</sup> F. Wei,<sup>48</sup> A.S. White,<sup>42</sup> C.P. Wong,<sup>20,36</sup> C.L. Woody,<sup>7</sup> M. Wysocki,<sup>51</sup>  
B. Xia,<sup>50</sup> L. Xue,<sup>20</sup> C. Xu,<sup>48</sup> Q. Xu,<sup>67</sup> S. Yalcin,<sup>62</sup> Y.L. Yamaguchi,<sup>11,62</sup> H. Yamamoto,<sup>66</sup> A. Yanovich,<sup>23</sup>  
I. Yoon,<sup>60</sup> J.H. Yoo,<sup>32</sup> I.E. Yushmanov,<sup>33</sup> H. Yu,<sup>48,53</sup> W.A. Zajc,<sup>13</sup> A. Zelenski,<sup>6</sup> S. Zhou,<sup>10</sup> and L. Zou<sup>8</sup>

## (PHENIX Collaboration)

- <sup>1</sup>Abilene Christian University, Abilene, Texas 79699, USA
- <sup>2</sup>Department of Physics, Augustana University, Sioux Falls, South Dakota 57197, USA
- <sup>3</sup>Department of Physics, Banaras Hindu University, Varanasi 221005, India
- <sup>4</sup>Bhabha Atomic Research Centre, Bombay 400 085, India
- <sup>5</sup>Baruch College, City University of New York, New York, New York, 10010 USA
- <sup>6</sup>Collider-Accelerator Department, Brookhaven National Laboratory, Upton, New York 11973-5000, USA
- <sup>7</sup>Physics Department, Brookhaven National Laboratory, Upton, New York 11973-5000, USA
- <sup>8</sup>University of California-Riverside, Riverside, California 92521, USA
- <sup>9</sup>Charles University, Ovocný trh 5, Praha 1, 116 36, Prague, Czech Republic
- <sup>10</sup>Science and Technology on Nuclear Data Laboratory, China Institute of Atomic Energy, Beijing 102413, People's Republic of China
- <sup>11</sup>Center for Nuclear Study, Graduate School of Science, University of Tokyo, 7-3-1 Hongo, Bunkyo, Tokyo 113-0033, Japan
- <sup>12</sup>University of Colorado, Boulder, Colorado 80309, USA
- <sup>13</sup>Columbia University, New York, New York 10027 and Nevis Laboratories, Irvington, New York 10533, USA
- <sup>14</sup>Czech Technical University, Žitkova 4, 166 36 Prague 6, Czech Republic
- <sup>15</sup>Debrecen University, H-4010 Debrecen, Egyetem tér 1, Hungary
- <sup>16</sup>ELTE, Eötvös Loránd University, H-1117 Budapest, Pázmány P. s. 1/A, Hungary
- <sup>17</sup>Ewha Womans University, Seoul 120-750, Korea
- <sup>18</sup>Florida A&M University, Tallahassee, FL 32307, USA
- <sup>19</sup>Florida State University, Tallahassee, Florida 32306, USA
- <sup>20</sup>Georgia State University, Atlanta, Georgia 30303, USA
- <sup>21</sup>Hiroshima University, Kagamiyama, Higashi-Hiroshima 739-8526, Japan
- <sup>22</sup>Department of Physics and Astronomy, Howard University, Washington, DC 20059, USA
- <sup>23</sup>IHEP Protvino, State Research Center of Russian Federation, Institute for High Energy Physics, Protvino, 142281, Russia
- <sup>24</sup>University of Illinois at Urbana-Champaign, Urbana, Illinois 61801, USA
- <sup>25</sup>Institute for Nuclear Research of the Russian Academy of Sciences, prospekt 60-letiya Oktyabrya 7a, Moscow 117312, Russia
- <sup>26</sup>Institute of Physics, Academy of Sciences of the Czech Republic, Na Slovance 2, 182 21 Prague 8, Czech Republic
- <sup>27</sup>Iowa State University, Ames, Iowa 50011, USA
- <sup>28</sup>Advanced Science Research Center, Japan Atomic Energy Agency, 2-4 Shirakata Shirane, Tokai-mura, Naka-gun, Ibaraki-ken 319-1195, Japan
- <sup>29</sup>Jeonbuk National University, Jeonju, 54896, Korea
- <sup>30</sup>Helsinki Institute of Physics and University of Jyväskylä, P.O.Box 35, FI-40014 Jyväskylä, Finland
- <sup>31</sup>KEK, High Energy Accelerator Research Organization, Tsukuba, Ibaraki 305-0801, Japan
- <sup>32</sup>Korea University, Seoul 02841, Korea
- <sup>33</sup>National Research Center "Kurchatov Institute", Moscow, 123098 Russia
- <sup>34</sup>Kyoto University, Kyoto 606-8502, Japan
- <sup>35</sup>Lawrence Livermore National Laboratory, Livermore, California 94550, USA
- <sup>36</sup>Los Alamos National Laboratory, Los Alamos, New Mexico 87545, USA
- <sup>37</sup>Department of Physics, Lund University, Box 118, SE-221 00 Lund, Sweden
- <sup>38</sup>IPNL, CNRS/IN2P3, Univ Lyon, Université Lyon 1, F-69622, Villeurbanne, France
- <sup>39</sup>University of Maryland, College Park, Maryland 20742, USA
- <sup>40</sup>Department of Physics, University of Massachusetts, Amherst, Massachusetts 01003-9337, USA
- <sup>41</sup>MATE, Laboratory of Femtoscopy, Károly Róbert Campus, Gyöngyös, Hungary
- <sup>42</sup>Department of Physics, University of Michigan, Ann Arbor, Michigan 48109-1040, USA
- <sup>43</sup>Mississippi State University, Mississippi State, Mississippi 39762, USA
- <sup>44</sup>Muhlenberg College, Allentown, Pennsylvania 18104-5586, USA
- <sup>45</sup>Nara Women's University, Kita-uoya Nishi-machi Nara 630-8506, Japan
- <sup>46</sup>National Research Nuclear University, MEPhI, Moscow Engineering Physics Institute, Moscow, 115409, Russia
- <sup>47</sup>University of New Mexico, Albuquerque, New Mexico 87131, USA
- <sup>48</sup>New Mexico State University, Las Cruces, New Mexico 88003, USA
- <sup>49</sup>Physics and Astronomy Department, University of North Carolina at Greensboro, Greensboro, North Carolina 27412, USA
- <sup>50</sup>Department of Physics and Astronomy, Ohio University, Athens, Ohio 45701, USA
- <sup>51</sup>Oak Ridge National Laboratory, Oak Ridge, Tennessee 37831, USA
- <sup>52</sup>IPN-Orsay, Univ. Paris-Sud, CNRS/IN2P3, Université Paris-Saclay, BP1, F-91406, Orsay, France
- <sup>53</sup>Peking University, Beijing 100871, People's Republic of China
- <sup>54</sup>PNPI, Petersburg Nuclear Physics Institute, Gatchina, Leningrad region, 188300, Russia
- <sup>55</sup>Pusan National University, Pusan 46241, Korea
- <sup>56</sup>RIKEN Nishina Center for Accelerator-Based Science, Wako, Saitama 351-0198, Japan
- <sup>57</sup>RIKEN BNL Research Center, Brookhaven National Laboratory, Upton, New York 11973-5000, USA
- <sup>58</sup>Physics Department, Rikkyo University, 3-34-1 Nishi-Ikebukuro, Toshima, Tokyo 171-8501, Japan
- <sup>59</sup>Saint Petersburg State Polytechnic University, St. Petersburg, 195251 Russia
- <sup>60</sup>Department of Physics and Astronomy, Seoul National University, Seoul 151-742, Korea

- <sup>61</sup>Chemistry Department, Stony Brook University, SUNY, Stony Brook, New York 11794-3400, USA  
<sup>62</sup>Department of Physics and Astronomy, Stony Brook University, SUNY, Stony Brook, New York 11794-3800, USA  
<sup>63</sup>University of Tennessee, Knoxville, Tennessee 37996, USA  
<sup>64</sup>Texas Southern University, Houston, TX 77004, USA  
<sup>65</sup>Department of Physics, Tokyo Institute of Technology, Oh-okayama, Meguro, Tokyo 152-8551, Japan  
<sup>66</sup>Tomonaga Center for the History of the Universe, University of Tsukuba, Tsukuba, Ibaraki 305, Japan  
<sup>67</sup>Vanderbilt University, Nashville, Tennessee 37235, USA  
<sup>68</sup>Weizmann Institute, Rehovot 76100, Israel  
<sup>69</sup>Institute for Particle and Nuclear Physics, Wigner Research Centre for Physics, Hungarian Academy of Sciences (Wigner RCP, RMKI) H-1525 Budapest 114, POBox 49, Budapest, Hungary  
<sup>70</sup>Yonsei University, IPAP, Seoul 120-749, Korea  
<sup>71</sup>Department of Physics, Faculty of Science, University of Zagreb, Bijenička c. 32 HR-10002 Zagreb, Croatia  
<sup>72</sup>Department of Physics, School of Natural Sciences, University of Zambia, Great East Road Campus, Box 32379, Lusaka, Zambia  
<sup>73</sup>debrecen

(Dated: July 27, 2022)

Small nuclear collisions are mainly sensitive to cold-nuclear-matter effects; however, the collective behavior observed in these collisions shows a hint of hot-nuclear-matter effects. The identified-particle spectra, especially the  $\phi$  mesons which contain strange and antistrange quarks and have a relatively small hadronic-interaction cross section, are a good tool to study these effects. The PHENIX experiment has measured  $\phi$  mesons in a specific set of small collision systems  $p$ +Al,  $p$ +Au, and  $^3\text{He}$ +Au, as well as  $d$ +Au [Phys. Rev. C **83**, 024909 (2011)], at  $\sqrt{s_{NN}} = 200$  GeV. The transverse-momentum spectra and nuclear-modification factors are presented and compared to theoretical-model predictions. The comparisons with different calculations suggest that quark-gluon plasma may be formed in these small collision systems at  $\sqrt{s_{NN}} = 200$  GeV. However, the volume and the lifetime of the produced medium may be insufficient for observing strangeness-enhancement and jet-quenching effects. The comparison with calculations suggests that the main production mechanisms of  $\phi$  mesons at midrapidity may be different in  $p$ +Al versus  $p/d/{}^3\text{He}$ +Au collisions at  $\sqrt{s_{NN}} = 200$  GeV. While thermal quark recombination seems to dominate in  $p/d/{}^3\text{He}$ +Au collisions, fragmentation seems to be the main production mechanism in  $p$ +Al collisions.

## I. INTRODUCTION

Quantum chromodynamics (QCD) predicts the existence of a state of matter, called the quark gluon plasma (QGP) where quarks and gluons are unbounded, at either high temperature or high baryon density. Relativistic ion collisions provide unique opportunities to study properties and characteristics of the QGP in laboratory experiments, which is one of the main goals of the PHENIX experiment [1]. The experimental evidences of formation of QGP at  $\sqrt{s_{NN}} = 200$  GeV have been observed in large collision systems such as Au+Au and Cu+Cu [2], while the observables in  $p$ + $p$  collisions are consistent with perturbative QCD (pQCD) calculations which describe primordial processes. The specific set of small collision systems available at the Relativistic Heavy Ion Collider (RHIC) at  $\sqrt{s_{NN}} = 200$  GeV provides an opportunity to investigate the minimal conditions (temperature and/or baryon density) sufficient for QGP formation.

It is believed (e.g., see Ref. [1]) that in small collision systems (such as  $p$ +Al,  $p$ +Au,  $d$ +Au, and  $^3\text{He}$ +Au), where energy and/or baryon density are not high enough to form a QGP, multiparticle production in the final state may occur without a QCD phase transition. The

cold-nuclear-matter effects [3, 4] seem to play a predominant role in small-system collisions at  $\sqrt{s_{NN}} = 200$  GeV. These effects include multiple-parton scattering, nuclear absorption and modification of the initial parton-distribution functions (PDFs) in nuclei. However, recent studies on elliptic and triangular flow in small systems suggest that QGP could be produced in  $p/d/{}^3\text{He}$ +Au collisions [5]. The flow measurements are well-explained by hydrodynamic model and are consistent with QGP droplet formation [6].

Additionally, the studies of  $J/\psi$  [7],  $\psi(2S)$  [8], and charged-hadron [9, 10] production at backward rapidity provide evidences of final-state effects not only in  $p/d/{}^3\text{He}$ +Au, but also in  $p$ +Al collisions. Nonetheless, these effects are weaker in  $p$ +Al, than in  $p/d/{}^3\text{He}$ +Au collisions.

The enhanced production of strange or hidden-strange hadrons in high-energy heavy-ion collisions, as compared to the appropriately scaled  $p$ + $p$  collisions, is a direct consequence of the process of chemical equilibration of strange quarks in QGP [11]. Thus, measurement of hadrons containing (anti)strange quarks has been established as a promising method of detecting the QGP. Recently published ratios of strange to nonstrange hadron yields observed at the Large Hadron Collider [12] show a smooth transition from elementary  $p$ + $p$  collisions at the higher center-of-mass energy of  $\sqrt{s_{NN}} = 7$  TeV, via  $p$ +Pb collisions at  $\sqrt{s_{NN}} = 5.02$  TeV, to heavy ion Pb+Pb colli-

\* Deceased

† PHENIX Spokesperson: akiba@rcf.rhic.bnl.gov

sions at lower energy  $\sqrt{s_{NN}} = 2.76$  TeV, when studies as a function of the charged-particle multiplicity,  $\langle dN_{ch}/d\eta \rangle$ . This observation is interpreted as possible QGP formation in  $p+p$  or  $p+Pb$  collisions at high enough  $\langle dN_{ch}/d\eta \rangle$  and demonstrates strangeness enhancement as a useful tool to study the onset of QGP formation. At RHIC, the strangeness enhancement in  $d+Au$  collisions at  $\sqrt{s_{NN}} = 200$  GeV is observed only in the Au-going direction ( $-2.2 < y < -1.2$ ) at  $2 < p_T < 5$  GeV/ $c$ , while in the  $d$ -going direction and at midrapidity, this effect is not observed within the uncertainties [2, 13]. Further measurements of strangeness enhancement in a broad set of small collision systems may provide an advantageous probe of QGP formation.

The strange-hadron yields also provide an additional degree of freedom, flavor, number of quarks, and mass, in the study of hadron production at high transverse momentum ( $p_T$ ). The energy loss of hard-scattered partons in the QGP, called jet quenching, manifests itself as a suppression of hadron production at high  $p_T$  in relativistic ion collisions as compared to the expectations from elementary proton-proton collisions [14]. The observation of both jet-quenching and strangeness-enhancement effects in various large systems (Au+Au and Cu+Cu collisions at  $\sqrt{s_{NN}} = 200$  GeV [2]) suggests that QGP can be formed in such collisions. By now, in central collisions, the  $\phi$  meson is less suppressed than other light-meson yields in the intermediate  $p_T$  range (2–5 GeV/ $c$ ) whereas at higher  $p_T$  (>5 GeV/ $c$ ), all light mesons are suppressed in comparison to the  $p+p$  collisions and show similar suppression values [2]. Both strangeness enhancement and jet quenching observed in  $A+A$  collisions are consistent with QGP formation, but are still under-explored in small collision systems at midrapidity and require further scrutiny.

The  $\phi$  vector meson, which is the lightest nearly pure bound state of  $s$  and  $\bar{s}$  quarks [15] and measurable up to high  $p_T$ , is considered a good probe for the study of both jet-quenching and strangeness-enhancement effects in relativistic ion collisions. The interaction cross section of the  $\phi$  meson with nonstrange hadrons has a small value [16]. The data on coherent  $\phi$  meson photoproduction show that  $\sigma_{\phi N} \approx 10$  mb [17, 18]. Additionally, because the lifetime (42 fm/ $c$  [16]) is longer than the QGP ( $\approx 5$  fm/ $c$  [1]),  $\phi$  mesons will decay mostly outside of the hot and dense matter and its daughters will not have much time to rescatter in the hadronic phase. Therefore,  $\phi$ -meson production is expected to be less affected by the later-stage hadronic interactions in the evolution of the system formed in relativistic ion collisions. Consequently, properties of the  $\phi$  meson are primarily controlled by the conditions in the early partonic phase and, hence, can be considered a clean probe to investigate the properties of matter created in relativistic ion collisions. The  $\phi$  meson has a mass of  $\approx 1$  GeV [15] which is comparable to the mass of the lightest baryons, such as protons.

This paper presents invariant  $p_T$  spectra and nuclear-modification factors of  $\phi$  mesons in  $p+Al$ ,  $p+Au$ ,  $d+Au$ ,

and  $^3\text{He}+Au$  collisions at  $\sqrt{s_{NN}} = 200$  GeV. The comparisons of obtained results to previous light-hadron-production measurements in small systems and to different model calculations are provided for better understanding of the underlying processes.

## II. DATA ANALYSIS

A detailed description of the PHENIX experimental set-up can be found elsewhere [19]. The beam-beam counters (BBC) [20] are used for the centrality definition, the determination of collision vertex along the beam axis (the  $z$ -vertex), and the event start time. The BBCs cover the pseudorapidity range  $3.0 < |\eta| < 3.9$ . The minimum-bias (MB) interaction trigger is also provided by the BBCs by requiring at least one inelastic nucleon-nucleon collision with the simultaneous detection of charged particles in both south BBC (Au[Al]-going direction) and north BBC ( $p$ [ $^3\text{He}$ ]-going direction). The event vertex is required to be within  $|z_{\text{vertex}}| < 30$  cm of the nominal interaction region.

Two central arms (east and west) of the PHENIX detector are used for electron, photon, and charged-hadron measurements. They each cover  $|\eta| < 0.35$  in pseudorapidity and  $90^\circ$  in azimuthal angle. The central arms include a particle-tracking system [21], which comprises drift chambers and pad chambers.

Charged particle identification (PID) is performed by simultaneous measurement of momentum, flight time, and path-length. The flight time is measured by the time-of-flight detector in the east part of the central arm spectrometer (TOF-E) [22, 23].

The data sets used in the analysis are collected from  $p+Al$  and  $p+Au$  collisions by the PHENIX detector in 2015 and  $^3\text{He}+Au$  collisions collected in 2014 at center-of-mass energy  $\sqrt{s_{NN}} = 200$  GeV. The integrated luminosities of the data sets used in this analysis are  $1.27$  pb $^{-1}$  in  $p+Au$ ,  $3.87$  pb $^{-1}$  in  $p+Al$ , and  $134$  nb $^{-1}$  in  $^3\text{He}+Au$  collisions.

Centrality selection is performed with the BBCs using the Glauber Monte Carlo procedure described in [24], wherein the charge in the BBCs is assumed to be proportional to the number of participating nucleons  $\langle N_{\text{part}} \rangle$ . In the current study, the distributions measured in the south BBC are used, which is the direction of the larger nucleus (Al or Au). The BBC charge is assumed to follow a negative-binomial distribution (NBD) with a mean of  $\langle N_{\text{part}} \rangle$  and the remaining NBD parameters determined from a  $\chi^2$  minimization of the combined Glauber+NBD calculation with respect to the data. The BBC distributions are divided into equal probability bins, and the corresponding Glauber distributions are used to calculate  $\langle N_{\text{part}} \rangle$  as well as the number of binary nucleon-nucleon collisions  $\langle N_{\text{coll}} \rangle$ , which are shown in Table I.

The determination of hadron yields in centrality bins has a known bias effect (see Ref. [25]). This effect results from the diffractive portion of the  $p+p$  collision, con-

TABLE I. Summary of the  $\langle N_{\text{coll}} \rangle$ ,  $\langle N_{\text{part}} \rangle$ , and  $f_{\text{bias}}$  values calculated using Glauber Monte Carlo simulation.

Collision	Centrality	$\langle N_{\text{coll}} \rangle$	$\langle N_{\text{part}} \rangle$	$f_{\text{bias}}$
$p+\text{Al}$	0%–72%	$2.1 \pm 0.1$	$3.1 \pm 0.1$	$0.80 \pm 0.02$
	0%–20%	$3.4 \pm 0.3$	$4.4 \pm 0.3$	$0.81 \pm 0.01$
	20%–40%	$2.3 \pm 0.1$	$3.3 \pm 0.1$	$0.90 \pm 0.02$
	40%–72%	$1.6 \pm 0.1$	$2.6 \pm 0.1$	$1.05 \pm 0.04$
$p+\text{Au}$	0%–84%	$4.7 \pm 0.3$	$5.7 \pm 0.3$	$0.86 \pm 0.01$
	0%–20%	$8.2 \pm 0.5$	$9.2 \pm 0.5$	$0.90 \pm 0.01$
	20%–40%	$6.1 \pm 0.4$	$7.1 \pm 0.4$	$0.98 \pm 0.01$
	40%–84%	$3.4 \pm 0.2$	$4.4 \pm 0.2$	$1.01 \pm 0.04$
${}^3\text{He}+\text{Au}$	0%–88%	$10.4 \pm 0.7$	$11.4 \pm 0.5$	$0.89 \pm 0.01$
	0%–20%	$22.3 \pm 1.7$	$21.1 \pm 1.3$	$0.95 \pm 0.01$
	20%–40%	$14.8 \pm 1.1$	$15.4 \pm 0.9$	$1.01 \pm 0.01$
	40%–60%	$8.4 \pm 0.6$	$9.5 \pm 0.6$	$1.02 \pm 0.01$
	60%–88%	$3.4 \pm 0.3$	$4.6 \pm 0.3$	$1.03 \pm 0.05$

stituent  $p+\text{Al}$  or  $p/d/{}^3\text{He}+\text{Au}$  collision, and manifests itself as a bias towards nondiffractive collisions, where higher charge is deposited in the BBC, and hence towards larger centrality. Increased trigger efficiency is correlated with a 1.55 times larger BBC multiplicity [9]. Bias effects were removed via correction factors  $f_{\text{bias}}$  that are calculated using a Glauber+NBD approach and following the detailed procedure described in Ref. [25].

The  $\phi$ -meson-production measurement is conducted via the kaon ( $K$ -meson) decay channel. The values of  $\phi$  meson mass, width ( $\Gamma$ ) and branching ratio ( $\text{Br}$ ) of  $\phi \rightarrow K^+K^-$  decay can be found in [15].

Each charged track is paired with its opposite sign to reconstruct the invariant-mass spectrum in every selected centrality class and  $p_T$  bin. For every track, the three momentum components are determined with the help of the drift chambers and the first layer of the pad chambers. Then, the invariant mass and transverse momentum are calculated from the kinematics of two-particle decay. This, so called “no PID,” technique is used for all collisions for  $p_T > 2.2 \text{ GeV}/c$ . To increase the signal to background ratio for  $p_T < 2.2 \text{ GeV}/c$ , one of the tracks is required to be identified as a kaon. The requirements of the charged track to be a kaon is determined by the TOF-E detector. This so-called “one-kaon PID” is used for  $p_T < 2.2 \text{ GeV}/c$  in  $p+\text{Au}$  and  ${}^3\text{He}+\text{Au}$  collisions. Additionally, to provide a cross check of the results and for estimation of systematic uncertainties for  ${}^3\text{He}+\text{Au}$  collisions, both kaons were required to be identified (“two-kaons PID”). For  $p+\text{Al}$  collisions only the “no PID” technique is applied due to low statistics. Figure 1 shows examples of mass spectra obtained in  ${}^3\text{He}+\text{Au}$  collisions using the three methods.

Invariant-mass spectra for opposite sign pairs comprise the  $\phi$ -meson signal and the combinatorial background. The combinatorial background comprises correlated and uncorrelated parts. The event-mixing technique [26] is applied in order to subtract the uncorrelated background.

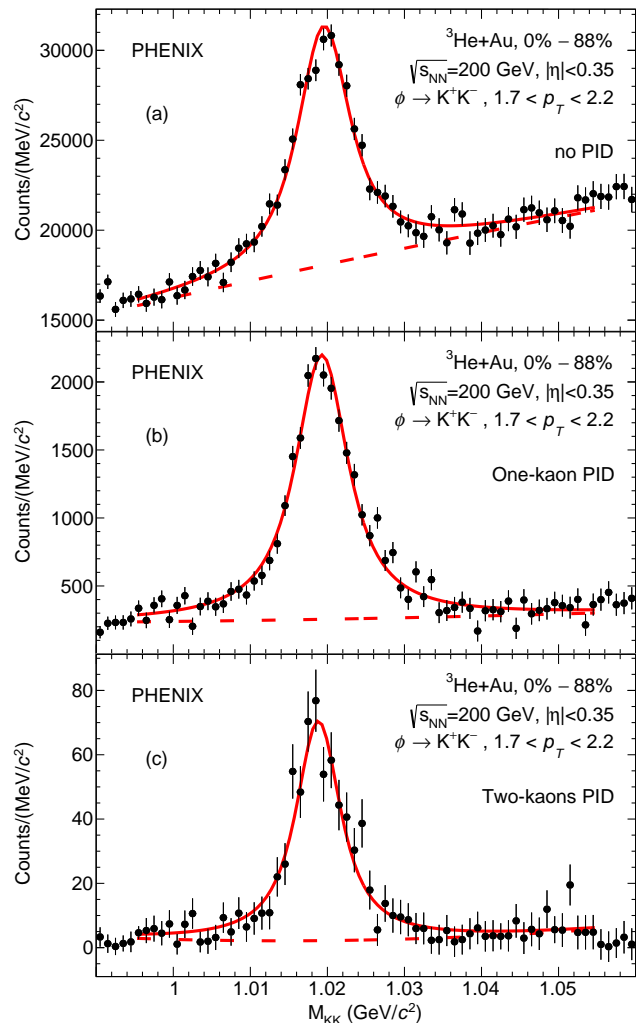


FIG. 1. Examples of invariant-mass distributions for the  $K^+K^-$  pairs in  ${}^3\text{He}+\text{Au}$  collisions at  $\sqrt{s_{NN}} = 200 \text{ GeV}$ , obtained with the (a) no PID, (b) one-kaon PID, and (c) two-kaons PID methods after subtraction of the combinatorial background estimated using the event-mixing technique. Plots correspond to integrated  $p_T$  for  $1.7 < p_T < 2.2 \text{ GeV}/c$ . Spectra are fitted to the sum of a Breit-Wigner function convoluted with a Gaussian function to account for the  $\phi$  signal, and a polynomial function to account for the residual background.

After subtraction, the background invariant-mass distribution is fitted with a Gaussian function convoluted with Breit-Wigner function to describe the signal and a second order polynomial function to describe the remaining correlated background from other particle decays ( $K_s^0 \rightarrow \pi^+\pi^-$ ,  $\Lambda \rightarrow p\pi^-$ ,  $\rho \rightarrow \pi^+\pi^-$ ,  $\omega \rightarrow \pi^0\pi^+\pi^-$  etc.). Gaussian  $\sigma$  value, corresponding to mass resolution, is constrained to the  $\sigma_{\text{exp}}$  value derived using a full GEANT [27] simulation of the PHENIX detector with zero natural width of  $\phi$  meson. The  $\Gamma$  parameter of the Breit-Wigner function is left as a free parameter in the fit of the simulated data, and its extracted value  $\Gamma_0$  is then used in the real data fitting to constrain the  $\Gamma$  parameter

to fall within  $\pm 10\%$  of the  $\Gamma_0$  value. The reconstruction efficiency ( $\varepsilon_{\text{rec}}$ ) of the  $\phi$  meson is determined using simulation with a  $\phi$  meson PDG width  $\Gamma$ . The raw yields of  $\phi$  mesons are obtained by integrating the invariant mass distribution in the range  $\pm 9$  MeV/ $c^2$  around the  $\phi$  meson mass after combinatorial background subtraction as shown in Fig. 1.

TABLE II. Type B systematic uncertainties on the  $\phi$  meson invariant yields in  $p$ +Al collisions at  $\sqrt{s_{NN}} = 200$  GeV

$p_T$ [GeV/ $c$ ]	1.45	3.45	3.95
Raw-yield extraction	18.1%	9.9%	11.2%
Acceptance	4.0%	4.0%	4.0%
Reconstruction efficiency	3.0%	3.0%	3.0%
Momentum scale	0.6%	3.0%	3.6%
Branching ratio	1.0%	1.0%	1.0%
Total type B	18.8%	11.5%	12.7%

TABLE III. Type B systematic uncertainties on the  $\phi$  meson invariant yields in  $p$ +Au collisions at  $\sqrt{s_{NN}} = 200$  GeV

$p_T$ [GeV/ $c$ ]	1.1	1.95	3.95
Raw-yield extraction	9.6%	8.8%	11.2%
Acceptance	5.0%	5.0%	5.0%
Reconstruction efficiency	4.0%	4.0%	4.0%
Momentum scale	0.5%	1.1%	3.6%
Branching ratio	1.0%	1.0%	1.0%
Total type B	11.6%	11.0%	13.4%

TABLE IV. Type B systematic uncertainties on the  $\phi$  meson invariant yields in  $^3\text{He}$ +Au collisions at  $\sqrt{s_{NN}} = 200$  GeV

$p_T$ [GeV/ $c$ ]	1.1	1.95	5.5	7.0
Raw-yield extraction	7.6%	6.8%	15.4%	14.8%
Acceptance	4.0%	4.0%	4.0%	4.0%
Reconstruction efficiency	3.0%	3.0%	3.0%	3.0%
Momentum scale	0.5%	1.1%	4.7%	5.0%
Branching ratio	1.0%	1.0%	1.0%	1.0%
Total type B	9.2%	8.6%	16.9%	16.4%

TABLE V. Type C systematic uncertainties on the  $\phi$  meson invariant yields in  $p$ +Al,  $p$ +Au, and  $^3\text{He}$ +Au collisions at  $\sqrt{s_{NN}} = 200$  GeV

	Centrality	0%–20%	40%–72%	0%–72%
$p$ +Al	Total type C	10.5%	9.2%	7.7%
$p$ +Au	Centrality	0%–20%	40%–84%	0%–84%
	Total type C	6.6%	7.4%	6.9%
$^3\text{He}$ +Au	Centrality	0%–20%	60%–88%	0%–88%
	Total type C	7.7%	10.1%	6.9%

The invariant spectra of  $\phi$  meson in each transverse-

momentum interval is calculated as

$$\frac{1}{2\pi N_{\text{event}}} \frac{d^2 N}{p_T dp_T dy} = \frac{f_{\text{bias}}}{2\pi p_T} \times \frac{N_{\text{raw}}}{N_{\text{event}} \text{Br} \cdot \varepsilon_{\text{rec}}(p_T) \Delta p_T \Delta y}, \quad (1)$$

where  $N_{\text{raw}}$  is the number of  $\phi$  mesons detected by the experimental setup (raw yield),  $N_{\text{event}}$  is the number of analyzed events, Br is the branching ratio of  $\phi \rightarrow K^+ K^-$  decay, and  $\varepsilon_{\text{rec}}(p_T)$  corrects for the limited acceptance of the detector and the  $\phi$  meson reconstruction efficiency.

Nuclear-modification factors are calculated as

$$R_{xA} = \frac{\sigma_{pp}^{\text{inel}}}{\langle N_{\text{coll}} \rangle} \cdot \frac{d^2 N_{xA}/dydp_T}{d^2 \sigma_{pp}/dydp_T}, \quad (2)$$

where  $d^2 N_{xA}/dydp_T$  is the per-event yield of particle production in  $x+A$  collisions,  $d^2 \sigma_{pp}/dydp_T$  is the production cross section in  $p+p$  collisions, and  $\sigma_{pp}^{\text{inel}} = 42.2$  mb [28] is the total inelastic proton-proton cross section. The  $p+p$  reference data used in the analysis is taken from [28].

There are three types of systematic uncertainties: type A (point-to-point uncorrelated); type B (point-to-point correlated), which can change the shape of the spectrum in a smooth way as a function of  $p_T$  and type C (global or normalization), which can only move all data points up or down by the same amount. The uncertainties of type A are dominated by the statistical precision of the data. Uncertainty of type B includes acceptance, reconstruction efficiency and momentum scale uncertainties, and uncertainty in the raw-yield extraction, which are evaluated by varying the identification approaches, fit parameters and the parameterization of the residual background. The trend in raw yield extraction uncertainty values at low  $p_T$  is mostly driven by the increasing signal to background ratio with increasing  $p_T$ , and at high  $p_T$  by worsening detector mass resolution and lower statistics. The various normalization correction terms have type C uncertainties. Uncertainty of type C includes  $\langle N_{\text{coll}} \rangle$ ,  $f_{\text{bias}}$  uncertainties, uncertainty caused by event overlap (0.9% for  $^3\text{He}$ +Au, 2.2% for  $p$ +Au, and 5.5% for  $p$ +Al), which might arise during the same bunch crossing, and uncertainty in normalization for the  $p+p$  cross section equal to  $\approx 9.7\%$ . The uncertainties are examined in each centrality class for  $p$ +Al,  $p$ +Au, and  $^3\text{He}$ +Au collisions and are found to be consistent among all centrality classes.

Tables II, III, and IV present typical values of the estimated type-B systematic uncertainties and Table V shows those for type C. In all three systems, the total systematic error is dominated by raw-yield extraction uncertainty.

### III. RESULTS

Figure 2 shows the invariant transverse momentum spectra of  $\phi$  mesons in  $p$ +Al,  $p$ +Au and  $^3\text{He}$ +Au collisions at  $\sqrt{s_{NN}} = 200$  GeV at midrapidity  $|\eta| < 0.35$ ,

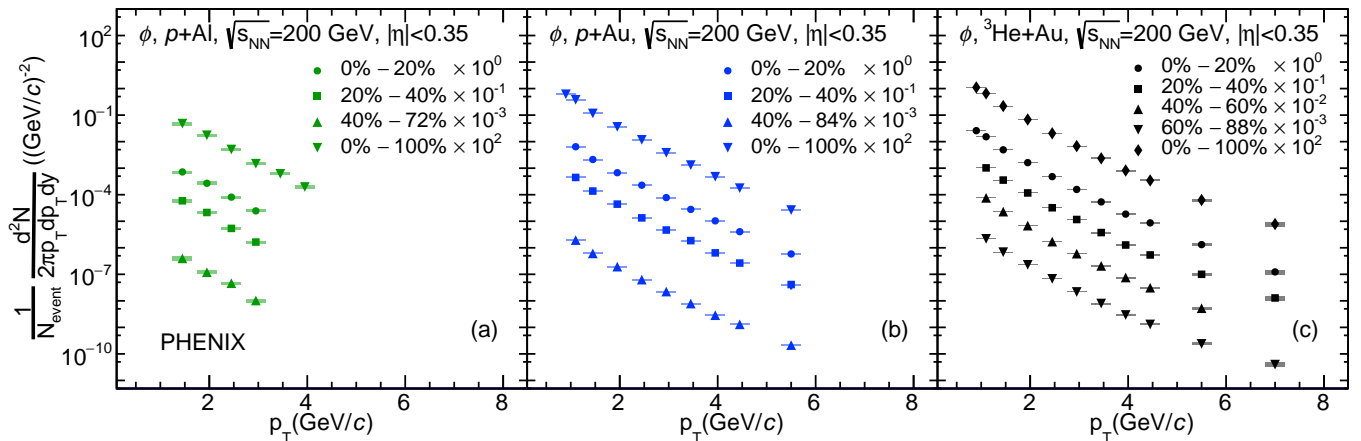


FIG. 2. Invariant transverse momentum spectra measured for  $\phi$  mesons in (a)  $p$ +Al, (b)  $p$ +Au and (c)  ${}^3\text{He}$ +Au collisions at  $\sqrt{s_{NN}} = 200$  GeV at midrapidity. The statistical uncertainties are shown by vertical bars, which are smaller than the size of the symbols, and the systematic uncertainties are indicated by rectangles, which are depicted wide to make them visible.

in four centrality bins in  $p$ +Al and  $p$ +Au and for five centrality bins in  ${}^3\text{He}$ +Au collisions.

Figure 3 shows  $\phi$  meson nuclear-modification factors  $R_{xA}$  measured in  $p$ +Al,  $p$ +Au,  $d$ +Au and  ${}^3\text{He}$ +Au collisions at  $\sqrt{s_{NN}} = 200$  GeV at midrapidity. The normalization uncertainty from  $p$ + $p$  ( $\approx 9.7\%$ ) is not shown [28]. From comparing  $p$ +Al,  $p$ +Au,  $d$ +Au and  ${}^3\text{He}$ +Au results, an ordering of  $\phi$ -meson  $R_{xA}$  might be seen in the intermediate  $p_T$  range in the most-central (0%–20%) and MB (0%–100%) collisions:  $R_{3\text{HeAu}} < R_{dAu} < R_{pAu}$ . Also at high  $p_T$ , a hint of suppression in central collisions, and a hint of enhancement in peripheral collisions is observed. Nonetheless, the  $\phi$ -meson  $R_{xA}$  are equal to unity within large uncertainties. Similar results were previously obtained for  $\pi^0$  production in small collision systems and was explained by conservation of energy [29]. The production of high-energy particles (with a large transverse momentum), by virtue of the conservation of energy, leads to a decrease in multiplicity in the collision [30] and hence [25] possibly incorrectly categorizing some central collisions as peripheral collisions. This effect might cause, at high  $p_T$ , a hint of  $R_{xA}$  suppression in central collisions and a hint of  $R_{xA}$  enhancement in peripheral collisions. This suggests that conclusions about energy loss in small collision systems cannot be drawn due to insufficient experimental precision and further careful theoretical treatment is required.

Figure 4 shows the comparison of  $\phi$  meson and  $\pi^0$ -meson nuclear-modification factors [29] measured in  $p$ +Al,  $p$ +Au,  $d$ +Au [2], and  ${}^3\text{He}$ +Au collisions at  $\sqrt{s_{NN}} = 200$  GeV at midrapidity. Because  $\phi$  meson contains  $s$  and  $\bar{s}$  quarks and  $\pi^0$  comprises of  $u$  and  $d$  quarks, this comparison can reveal the possible strangeness enhancement effect. Panels (a) to (d) show the results for the most central collisions and panels (e) to (h) show the results for the most peripheral collisions. In the  $\phi$  meson  $p_T$ -range up to 8.0 GeV/ $c$ ,  $\phi$  and  $\pi^0$ -mesons nuclear-modification factors are in agreement within their uncer-

tainties for the different collision systems. The  $\phi$  meson production in the most central collisions shows a trend to less suppression or larger enhancement than the  $\pi^0$  meson production at moderate  $p_T$ , however it cannot be concluded due to large systematic uncertainties. In heavy ion collisions (Au+Au and Cu+Cu), in the most central collisions, the  $\phi$  meson  $R_{xA}$  shows less suppression than  $\pi^0$ -meson in the intermediate  $p_T$  range of  $2 < p_T$  (GeV/ $c$ )  $< 5$  [2]. This result is qualitatively consistent with quark coalescence from QGP models [31, 32]. The observation of strangeness enhancement in small collision systems at midrapidity cannot be concluded due to large systematic uncertainties.

To separate collective and noncollective phenomena and to study the  $\phi$  meson production mechanism, the data are compared to calculations using PYTHIA/Angantyr [33], Eskola-Paakkinen-Paukkunen-Salgado (EPPS16) [34], coordinated-theoretical-experimental project on QCD (NCTEQ15) nuclear PDF [35], and a multiphase transport (AMPT) [36] models for both default [def] and string-melting [sm].

PYTHIA8.303 [37] was developed based on leading-order pQCD calculations with soft-hadron production matching the observed data from  $p$ + $p$  collisions at different energies. To further develop its framework, Angantyr was created to include heavy ion collisions in the same PYTHIA framework without introducing a new state of matter (collective behavior).

The first step is to establish the inclusive hadron spectrum in  $p$ + $p$  collisions at  $\sqrt{s} = 200$  GeV from the PYTHIA8.303. Then, the  $\phi$  meson spectra were estimated from the PYTHIA/Angantyr in  $p$ +Al,  $p$ +Au,  $d$ +Au or  ${}^3\text{He}$ +Au collision at the same collision energy. The parameters used in the event generation of PYTHIA are listed in Table VII. The multiplication factor for multiparton interactions is introduced to match  $\eta$ -dependent multiplicity distribution in  $p$ + $p$  collisions at  $\sqrt{s_{NN}} = 200$  GeV in PYTHIA calculations and experimental data [38]. The

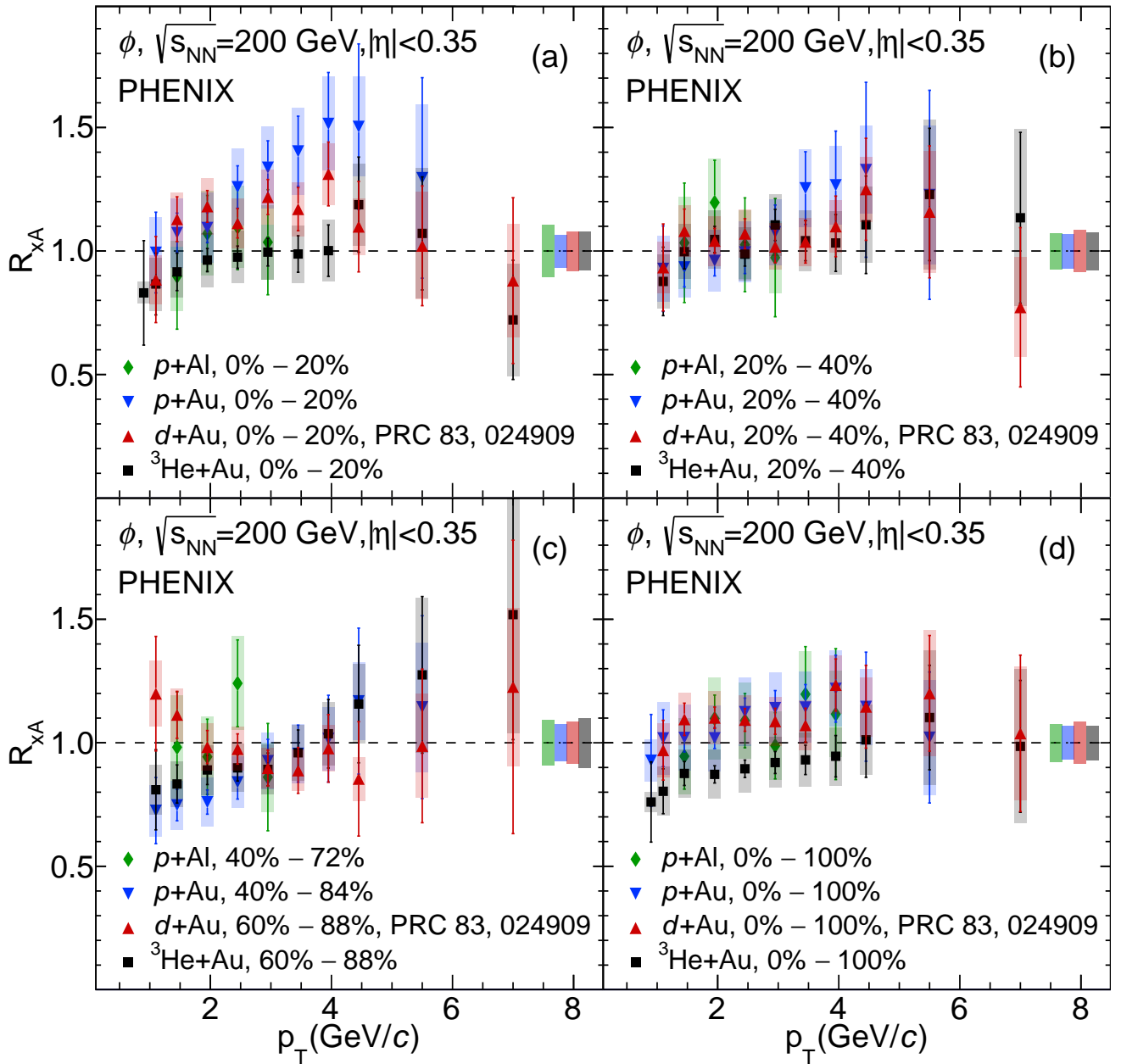


FIG. 3. Comparison of  $\phi$ -meson nuclear-modification factors in  $p$ +Al,  $p$ +Au,  $d$ +Au [2], and  ${}^3\text{He}$ +Au collisions at  $\sqrt{s_{NN}} = 200$  GeV at midrapidity. Here and in following figures, the statistical uncertainties are shown by vertical bars and the systematic uncertainties are indicated by rectangles, which are depicted wide to make them visible. The normalization uncertainty from  $p$ + $p$  of about 9.7% is not shown [28].

$R_{xA}$  were then calculated with the  $\langle N_{\text{coll}} \rangle$  values taken from PYTHIA/Angantyr, which are listed in Table VI.

TABLE VI.  $\langle N_{\text{coll}} \rangle$  values obtained from PYTHIA 8.303 [37].

$p$ +Al	$p$ +Au	$d$ +Au	${}^3\text{He}$ +Au
2.1	4.2	6.2	7.9

Systematic uncertainties for PYTHIA/Angantyr calcu-

lations include the uncertainty of the PDFs variation and uncertainty in total  $x$ +A cross section. Figure 5 shows the comparison of experimental results on  $\phi$  meson production in  $p$ +Al,  $p$ +Au,  $d$ +Au and  ${}^3\text{He}$ +Au at  $\sqrt{s_{NN}} = 200$  GeV to PYTHIA/Angantyr model predictions. The results shown for the MB collisions suggest that PYTHIA/Angantyr calculations describe the experimental results within uncertainties, however predict the reverse  $R_{xA}$  ordering:  $R_{pAu} < R_{dAu} < R_{{}^3\text{He}Au}$ . Despite the agreement of  $R_{xA}$  experimental values with PYTHIA/Angantyr calculations, the same calculations



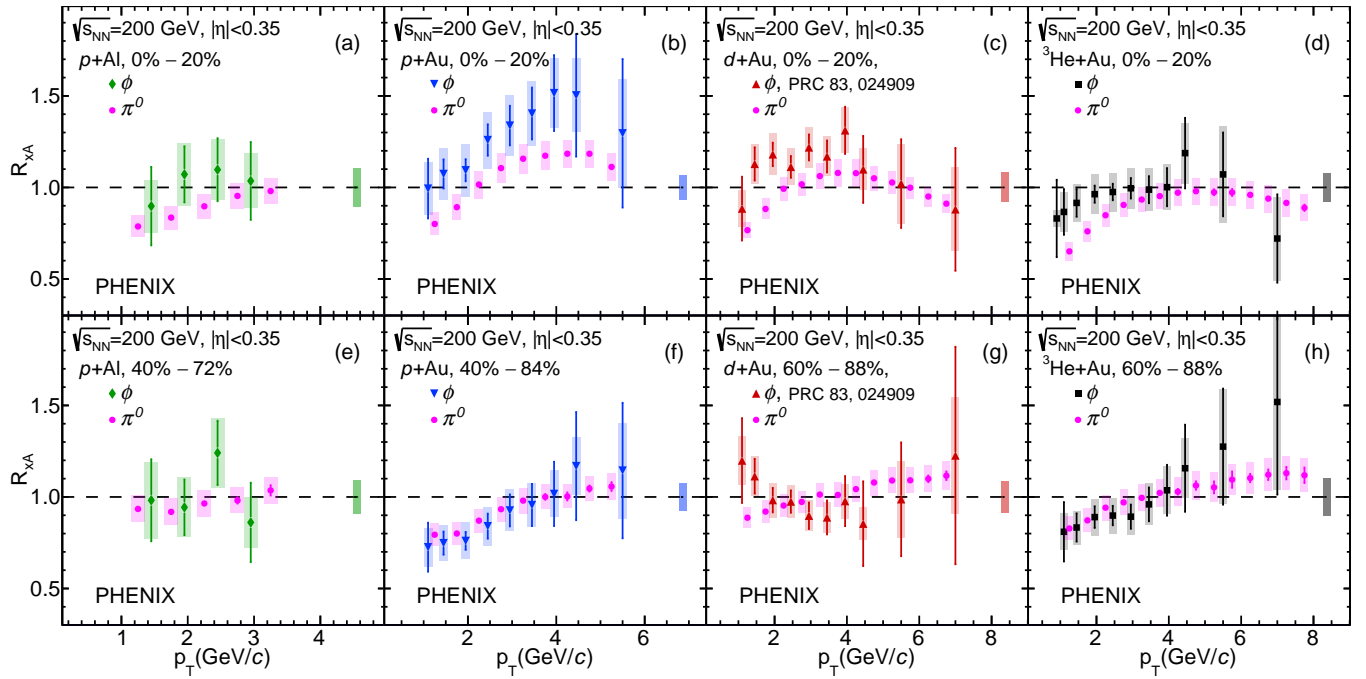


FIG. 4. The comparison of  $\phi$  meson to  $\pi^0$ -meson (from Ref. [29]) nuclear-modification factors in  $p+Al$ ,  $p+Au$ ,  $d+Au$  [2], and  ${}^3\text{He}+Au$  (a) to (d) central and (e) to (h) peripheral collisions at  $\sqrt{s_{NN}} = 200$  GeV at midrapidity. The normalization uncertainty from  $p+p$  ( $\approx 9.7\%$ ) is not shown.

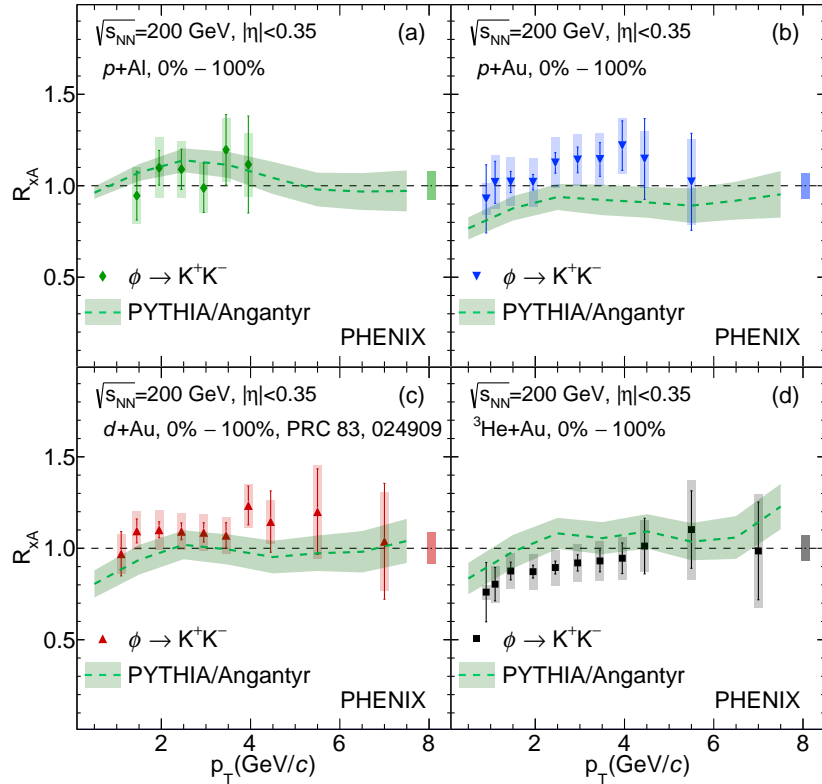


FIG. 5. Experimental results on  $\phi$  meson production in (a)  $p+Al$ , (b)  $p+Au$ , (c)  $d+Au$  [2], and (d)  ${}^3\text{He}+Au$  collisions at  $\sqrt{s_{NN}} = 200$  GeV at midrapidity ( $|\eta| < 0.35$ ) and comparisons to PYTHIA/Angantyr [33] model predictions.

have discrepancies with experimental results on the  $\phi$ -meson invariant- $p_T$  spectra in  $p+p$  [39] and all considered

systems at  $\sqrt{s_{NN}} = 200$  GeV at midrapidity.

Figure 6 shows the experimental data compared to calculations based on NCTEQ15 nPDF [35] and EPPS16 nPDF [34] interfaced with PYTHIA8.303. Both NCTEQ15, and EPPS16 nPDF results show conformity with experimental data within uncertainties. However, the nPDF calculations fail to predict the experimental ordering of  $\phi$  meson  $R_{xA}$  at moderate  $p_T$ , as was previously observed for  $\pi^0$  production. The different trends of the nPDF calculations compared to the experimental data suggest that the nuclear modification in  $p/d/{}^3\text{He}+\text{Au}$  collisions might involve some mechanism(s) additional to nPDF.

The AMPT model [36] includes the initial-partonic and final-hadronic matter, as well as the transition between the two phases. This model provides an opportunity to study the hadronization mechanism in relativistic ion collisions. In the AMPT-default model, only minijet partons from processes evaluated by the pQCD are involved in the Zhang's parton cascade [40] and are recombined with their parent strings when they stop interacting. The resulting strings are converted to hadrons using the Lund string fragmentation model.

In the extended-string-melting version of the AMPT model, the strings, formed in the nonperturbative processes, melt into partonic degrees of freedom and a quark-coalescence model [36] is used to combine partons into hadrons. The AMPT results were obtained using a parton-scattering cross section of 3.0 mb and incorporating the nuclear shadowing effect [36].

Figure 7 shows the comparison of experimental  $\phi$  meson invariant  $p_T$  spectra in MB  $p+\text{Al}$ ,  $p+\text{Au}$ ,  $d+\text{Au}$ , and  ${}^3\text{He}+\text{Au}$  collisions to the predictions of default and string-melting AMPT calculations. The  $p/d/{}^3\text{He}+\text{Au}$  results are well described in the frame of the string-melting version of the AMPT model. The ratios of  $\phi$ -meson yields, measured in the experiment to AMPT calculations, are consistent with each other in  $p/d/{}^3\text{He}+\text{Au}$  collisions and therefore, the AMPT model is able to predict the experimental ordering of  $\phi$  meson  $R_{xA}$ . The default version calculations underpredict the experimental data for  $p/d/{}^3\text{He}+\text{Au}$  collisions. In contrast, the string-melting version of the AMPT-model calculations seems to overpredict the  $\phi$ -meson invariant spectra in  $p+\text{Al}$  results, whereas the default-version calculations demonstrate more conformity. Therefore, the coalescence mechanism apparently plays a considerable role in hadronization in  $p/d/{}^3\text{He}+\text{Au}$  collisions at  $\sqrt{s_{NN}} = 200$  GeV. This confirms previous studies of light-hadron production at RHIC, where some of QGP effects such as baryon enhancement [41] and reversed mass ordering of  $v_2$  in small collision systems [42] have been interpreted in terms of recombination model of hadronization. However, the comparison of experimental data to theoretical model predictions in the current study suggests that in  $p+\text{Al}$  at midrapidity the contribution of the coalescence mechanism in  $\phi$  meson production is less significant.

#### IV. SUMMARY

In summary, PHENIX has measured  $\phi$  meson invariant transverse momentum spectra in  $|\eta| < 0.35$  in  $p+\text{Al}$ ,  $p+\text{Au}$  and  ${}^3\text{He}+\text{Au}$  collisions at  $\sqrt{s_{NN}} = 200$  GeV in the range  $1.0 < p_T < 4.2(6.25, 7.75)$  GeV/ $c$  for different centrality classes via the kaon decay channel. The nuclear-modification factors in these collision systems were also presented. These first measurements of  $\phi$  meson production and its nuclear modification in highly asymmetric small collision systems at RHIC fill the gaps in  $\phi$  meson measurements between previous results in  $p+p$ ,  $d+\text{Au}$ , and heavy-ion collisions.

In the most central and MB collisions in the intermediate  $p_T$  range  $\phi$  meson nuclear-modification factors show a hint of ordering:  $R_{{}^3\text{HeAu}} < R_{d\text{Au}} < R_{p\text{Au}}$ . In other centralities,  $\phi$  meson  $R_{xA}$  exhibit similar shape over all  $p_T$  range for all small systems. A hint of suppression in central collisions and a hint of enhancement in peripheral collisions at high- $p_T$  could be explained as events with high- $p_T$  mesons having smaller underlying event multiplicity.

The  $\phi$  meson production in the most central collisions shows a trend to less suppression than the  $\pi^0$  meson production at moderate  $p_T$ . However, the  $R_{xA}$  for both mesons are in agreement within uncertainties. This might suggest that strangeness-enhancement effects cannot be precluded.

Although the hot-nuclear-matter effects, such as strangeness enhancement and jet quenching, are imperceptible in small collision systems,  $\phi$  meson  $R_{xA}$  in  $p/d/{}^3\text{He}+\text{Au}$  collisions are in good agreement with the string-melting version of AMPT calculations, whereas the default version of AMPT calculations underpredict the data. Although PYTHIA/Angantyr and EPPS16 and NCTEQ15 nPDF calculations describe the experimental results within uncertainties, the predicted  $R_{xA}$  values do not describe measured  $R_{xA}$  ordering.

Experimental results in  $p+\text{Al}$  collisions are better described with the default version of the AMPT-model calculations and are also consistent with PYTHIA model and nPDFs calculations. Hence, in spite of some collective effects observed in  $p+\text{Al}$  collisions at  $\sqrt{s_{NN}} = 200$  GeV at backward rapidity, at midrapidity the QGP formation does not reveal itself.

The obtained results are in favor of the QGP formation in small collision systems. However, the volume and lifetime of the medium produced in these collisions might be insufficient for observing strangeness-enhancement and jet-quenching effects.

Comparisons with model predictions suggest, that  $\phi$ -meson production in  $p/d/{}^3\text{He}+\text{Au}$  collisions at  $\sqrt{s_{NN}} = 200$  GeV might be driven by mechanisms additional to nPDF. The hadronization process in  $p+\text{Al}$  collisions could be interpreted within the frame of the fragmentation model and the influence of a coalescence mechanism seems to be negligible at midrapidity. The larger  $p/d/{}^3\text{He}+\text{Au}$  systems can be well described by in-

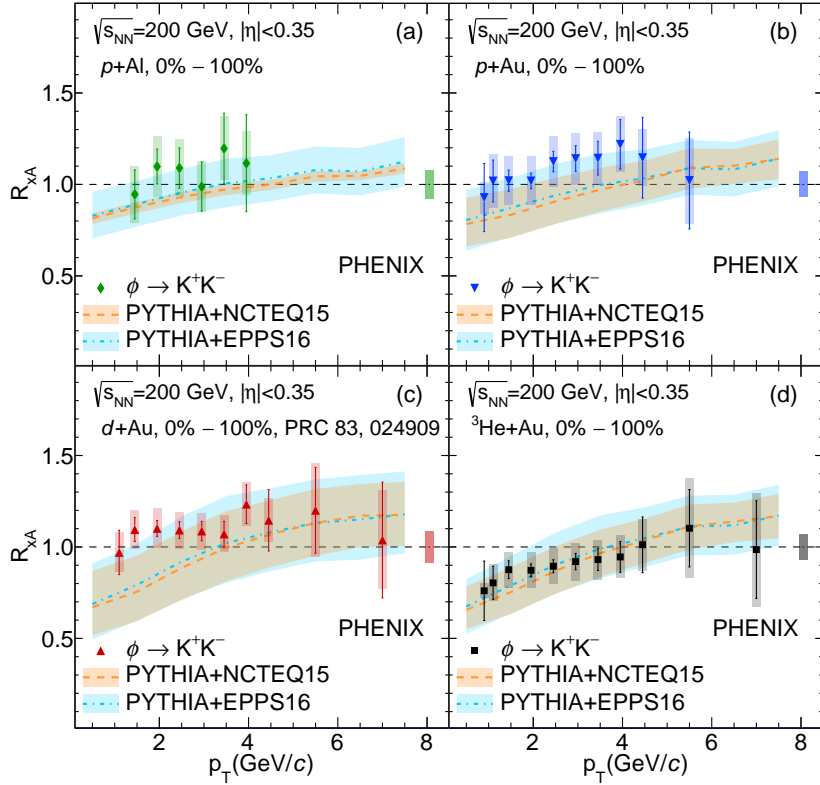


FIG. 6. Experimental results on  $\phi$ -meson production in (a)  $p$ +Al, (b)  $p$ +Au, (c)  $d$ +Au [2], and (d)  ${}^3\text{He}$ +Au collisions at  $\sqrt{s_{NN}} = 200$  GeV at midrapidity ( $|\eta| < 0.35$ ) and comparisons to EPPS16 [34] and NCTEQ15 [35] nuclear PDF calculations.

TABLE VII. Parameters used in PYTHIA

parameter	value	description
SoftQCD:	all = on	All soft QCD processes Used for PYTHIA /Angantyr calculations
	inelastic = on	All soft QCD processes, except for elastic Used for NCTEQ15+PYTHIA and EPPS16+PYTHIA calculations
PDF:pSet	8	CTEQ6L1 parton-distribution function
MultipartonInteractions:Kfactor	0.5	Multiplication factor for multiparton interaction

voking the coalescence mechanism. Further studies of QGP effects in small collision systems and comparison of all available experimental results to the theoretical predictions, considering hot- and cold-nuclear-matter effects, are necessary for revealing the possibility of QGP formation. Particularly, the comparison of obtained  $\phi$  meson results to  $p(\bar{p})$  production in small collision systems at  $\sqrt{s_{NN}} = 200$  GeV at midrapidity can reveal a role of recombination or radial flow in observed  $\phi$  and  $\pi^0$   $R_{xA}$  ordering.

## ACKNOWLEDGMENTS

We thank the staff of the Collider-Accelerator and Physics Departments at Brookhaven National Laboratory and the staff of the other PHENIX participating institutions for their vital contributions. We acknowledge support from the Office of Nuclear Physics in the Office of Science of the Department of Energy, the National Science Foundation, Abilene Christian University Research Council, Research Foundation of SUNY, and Dean of the College of Arts and Sciences, Vanderbilt University (USA), Ministry of Education, Culture, Sports, Science, and Technology and the Japan Society for the Promotion of Science (Japan), Natural Science Foundation of China (People's Republic of China), Croatian

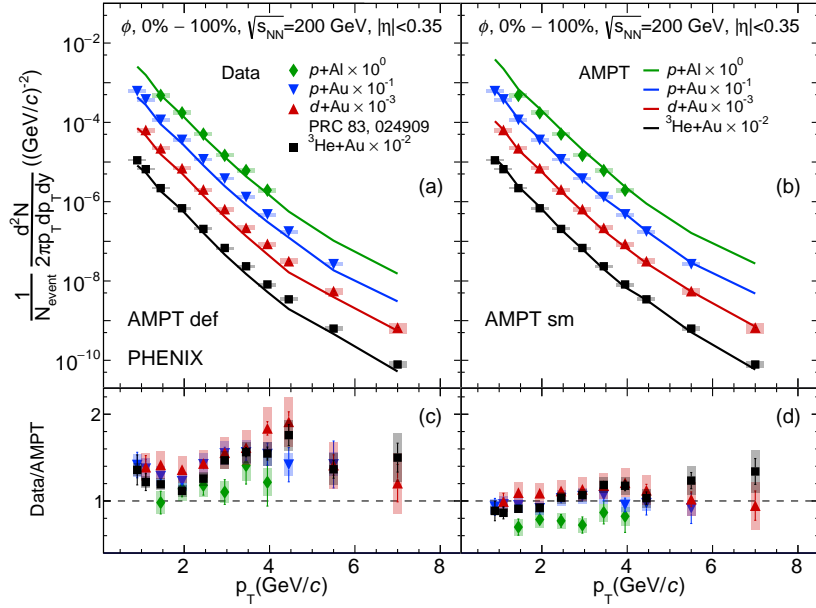


FIG. 7. Experimental results on  $\phi$  meson invariant  $p_T$  spectra in  $p$ +Al,  $p$ +Au,  $d$ +Au, and  ${}^3\text{He}$ +Au collisions at  $\sqrt{s_{NN}} = 200$  GeV at midrapidity ( $|\eta| < 0.35$ ) and comparisons to (a) default [def] and (b) string melting [sm] versions of the AMPT-model predictions. Panels (c) and (d) show data to AMPT-calculation ratios; the markers, error bars, and error boxes are the same as for panels (a) and (b).

Science Foundation and Ministry of Science and Education (Croatia), Ministry of Education, Youth and Sports (Czech Republic), Centre National de la Recherche Scientifique, Commissariat à l'Énergie Atomique, and Institut National de Physique Nucléaire et de Physique des Particules (France), J. Bolyai Research Scholarship, EFOP, the New National Excellence Program (ÚNKP), NKFIH, and OTKA (Hungary), Department of Atomic Energy and Department of Science and Technology (India), Israel Science Foundation (Israel), Basic Science Research and SRC(CENuM) Programs through NRF funded by

the Ministry of Education and the Ministry of Science and ICT (Korea), Ministry of Education and Science, Russian Academy of Sciences, Federal Agency of Atomic Energy (Russia), VR and Wallenberg Foundation (Sweden), University of Zambia, the Government of the Republic of Zambia (Zambia), the U.S. Civilian Research and Development Foundation for the Independent States of the Former Soviet Union, the Hungarian American Enterprise Scholarship Fund, the US-Hungarian Fulbright Foundation, and the US-Israel Binational Science Foundation.

- [1] K. Adcox *et al.*, Formation of dense partonic matter in relativistic nucleus-nucleus collisions at RHIC: Experimental evaluation by the PHENIX Collaboration, *Nucl. Phys. A* **757**, 184 (2005).
- [2] A. Adare *et al.*, Nuclear modification factors of  $\phi$  mesons in  $d$ +Au, Cu+Cu, and Au+Au collisions at  $\sqrt{s_{NN}} = 200$  GeV, *Phys. Rev. C* **83**, 024909 (2011).
- [3] C. O. Dorso, P. A. G. Molinelli, J. I. Nichols, and J. A. López, Cold nuclear matter, arXiv:1211.5582.
- [4] A. Adare *et al.* (PHENIX Collaboration),  $\phi$  meson production in  $d$ +Au collisions at  $\sqrt{s_{NN}} = 200$  GeV, *Phys. Rev. C* **92**, 044909 (2015).
- [5] C. Aidala *et al.* (PHENIX Collaboration), Creation of quark-gluon plasma droplets with three distinct geometries, *Nature Phys.* **15**, 214 (2019).
- [6] B. Schenke, C. Shen, and P. Tribedy, Hybrid Color Glass Condensate and hydrodynamic description of the Relativistic Heavy Ion Collider small system scan, *Phys. Lett. B* **803**, 135322 (2020).
- [7] U. A. Acharya *et al.* (PHENIX Collaboration), Measurement of  $J/\psi$  at forward and backward rapidity in  $p$ + $p$ ,  $p$ +Al,  $p$ +Au, and  ${}^3\text{He}$ +Au collisions at  $\sqrt{s_{NN}} = 200$  GeV, *Phys. Rev. C* **102**, 014902 (2020).
- [8] U. A. Acharya *et al.* (PHENIX Collaboration), Measurement of  $\psi(2S)$  nuclear modification at backward and forward rapidity in  $p$ + $p$ ,  $p$ +Al, and  $p$ +Au collisions at  $\sqrt{s_{NN}} = 200$  GeV, arXiv:2202.03863.
- [9] A. Adare *et al.* (PHENIX Collaboration), Pseudorapidity dependence of particle production and elliptic flow in asymmetric nuclear collisions of  $p$ +Al,  $p$ +Au,  $d$ +Au, and  ${}^3\text{He}$ +Au at  $\sqrt{s_{NN}} = 200$  GeV, *Phys. Rev. Lett.* **121**, 222301 (2018).
- [10] C. Aidala *et al.* (PHENIX Collaboration), Nuclear-modification factor of charged hadrons at forward and

- backward rapidity in  $p+Al$  and  $p+Au$  collisions at  $\sqrt{s_{NN}} = 200$  GeV, Phys. Rev. C **101**, 034910 (2020).
- [11] P. Koch, B. Muller, and J. Rafelski, Strangeness in Relativistic Heavy Ion Collisions, Phys. Rept. **142**, 167 (1986).
- [12] J. Adam *et al.* (ALICE Collaboration), Enhanced production of multi-strange hadrons in high-multiplicity proton-proton collisions, Nature Phys. **13**, 535 (2017).
- [13] A. Adare *et al.* (PHENIX Collaboration),  $\phi$  meson production in  $d+Au$  collisions at  $\sqrt{s_{NN}} = 200$  GeV, Phys. Rev. C **92**, 044909 (2015).
- [14] D. d'Énterria, 6.4 Jet quenching, Landolt-Börnstein, Group I, 471 (2010).
- [15] P. A. Zyla *et al.* (Particle Data Group), Reviews of Particle Physics, Prog. Theor. Exp. Phys. **2020**, 083C01 (2020).
- [16] A. Shor,  $\phi$ -meson production as a probe of the Quark-Gluon Plasma, Phys. Rev. Lett. **54**, 1122 (1985).
- [17] M. Nasim, V. Bairathi, M. K. Sharma, B. Mohanty, and A. Bhasin, A Review on  $\phi$  Meson Production in Heavy-Ion Collision, Adv. High Energy Phys. **2015**, 197930 (2015).
- [18] A. Sibirtsev, H.-W. Hammer, U.-G. Meissner, and A. W. Thomas,  $\phi$ -meson photoproduction from nuclei, Eur. Phys. J. A **29**, 209 (2006).
- [19] K. Adcox *et al.* (PHENIX Collaboration), PHENIX detector overview, Nucl. Instrum. Methods Phys. Res., Sec. A **499**, 469 (2003).
- [20] M. Allen *et al.*, PHENIX inner detectors, Nucl. Instrum. Methods Phys. Res., Sec. A **499**, 549 (2003), The Relativistic Heavy Ion Collider Project: RHIC and its Detectors.
- [21] K. Adcox *et al.*, PHENIX central arm tracking detectors, Nucl. Instrum. Methods Phys. Res., Sec. A **499**, 489 (2003), the Relativistic Heavy Ion Collider Project: RHIC and its Detectors.
- [22] L. Carlén *et al.*, A large-acceptance spectrometer for tracking in a high multiplicity environment, based on space point measurements and high resolution time-of-flight, Nucl. Instrum. Methods Phys. Res., Sec. A **431**, 123 (1999).
- [23] M. Aizawa *et al.* (PHENIX Collaboration), PHENIX central arm particle ID detectors, Nucl. Instrum. Methods Phys. Res., Sec. A **499**, 508 (2003).
- [24] M. L. Miller, K. Reygers, S. J. Sanders, and P. Steinberg, Glauber Modeling in High-Energy Nuclear Collisions, Ann. Rev. Nucl. and Part. Science **57**, 205 (2007).
- [25] A. Adare *et al.* (PHENIX Collaboration), Centrality categorization for  $R_{p(d)+A}$  in high-energy collisions, Phys. Rev. C **90**, 034902 (2014).
- [26] S. S. Adler *et al.*, Production of  $\phi$  mesons at midrapidity in  $\sqrt{s_{NN}} = 200$  GeV Au+Au collisions at relativistic energies, Phys. Rev. C **72**, 014903 (2005).
- [27] R. Brun, F. Bruyant, F. Carminati, S. Giani, M. Maire, A. McPherson, G. Patrick, and L. Urban, *GEANT Detector Description and Simulation Tool*, CERN Program Library ; W5013 (CERN Geneva, Switzerland, 1994) long Writeup W5013.
- [28] A. Adare *et al.* (PHENIX Collaboration), Measurement of neutral mesons in p+p collisions at  $\sqrt{s} = 200$  GeV and scaling properties of hadron production, Phys. Rev. D **83**, 052004 (2011).
- [29] U. A. Acharya *et al.* (PHENIX Collaboration), Systematic study of nuclear effects in  $p+Al$ ,  $p+Au$ ,  $d+Au$ , and  $^3He+Au$  collisions at  $\sqrt{s_{NN}} = 200$  GeV using  $\pi^0$  production (), arXiv:2111.05756.
- [30] M. Kordell and A. Majumder, Jets in  $d(p)$ -A Collisions: Color Transparency or Energy Conservation, Phys. Rev. C **97**, 054904 (2018).
- [31] V. Greco, C. M. Ko, and P. Lévai, Parton Coalescence and the Antiproton/Pion Anomaly at RHIC, Phys. Rev. Lett. **90**, 202302 (2003).
- [32] R. C. Hwa and C. B. Yang, Scaling behavior at high  $pt$  and the  $p/\pi$  ratio, Phys. Rev. C **67**, 034902 (2003).
- [33] A. Vieira da Silva, W. M. Serenone, D. D. Chinellato, J. Takahashi, and C. Bierlich, Studies of heavy-ion collisions using PYTHIA Angantyr and UrQMD (2020), arXiv:2002.10236.
- [34] K. J. Eskola, P. Paakkinen, H. Paukkunen, and C. A. Salgado, EPPS16: Nuclear parton distributions with LHC data, Eur. Phys. J. C **77**, 163 (2017).
- [35] K. Kovarič, A. Kusina, T. Ježo, D. B. Clark, C. Kappel, F. Lyonnet, J. G. Morfín, F. I. Olness, J. F. Owens, I. Schienbein, and J. Y. Yu, nCTEQ15: Global analysis of nuclear parton distributions with uncertainties in the CTEQ framework, Phys. Rev. D **93**, 085037 (2016).
- [36] Z.-W. Lin, C. M. Ko, B.-A. Li, B. Zhang, and S. Pal, Multiphase transport model for relativistic heavy ion collisions, Phys. Rev. C **72**, 064901 (2005).
- [37] T. Sjöstrand, S. Ask, J. R. Christiansen, R. Corke, N. Desai, P. Ilten, S. Mrenna, S. Prestel, C. O. Rasmussen, and P. Z. Skands, An introduction to PYTHIA8.2, Comp. Phys. Comm. **191**, 159 (2015).
- [38] B. Alver *et al.*, Charged-particle multiplicity and pseudorapidity distributions measured with the PHOBOS detector in Au+Au, Cu+Cu,  $d+Au$ , and  $p+p$  collisions at ultrarelativistic energies, Phys. Rev. C **83**, 024913 (2011).
- [39] Adam, J. and others,  $K^*(892)^0$  and  $\phi(1020)$  meson production at high transverse momentum in  $pp$  and Pb-Pb collisions at  $\sqrt{s_{NN}} = 2.76$  TeV, arXiv:1702.00555.
- [40] B. Zhang, ZPC 1.0.1: a parton cascade for ultrarelativistic heavy ion collisions, Comp. Phys. Comm. **109**, 193 (1998).
- [41] A. Adare *et al.*, Spectra and ratios of identified particles in Au+Au and  $d+Au$  collisions at  $\sqrt{s_{NN}} = 200$  GeV, Phys. Rev. C **88**, 024906 (2013).
- [42] A. Adare *et al.* (PHENIX Collaboration), Measurements of mass-dependent azimuthal anisotropy in central  $p+Au$ ,  $d+Au$ , and  $^3He+Au$  collisions at  $\sqrt{s_{NN}} = 200$  GeV, Phys. Rev. C **97**, 064904 (2018).